Low amplitude strain accumulation model for natural soft clays below railways

(article starts on next page)

Low amplitude strain accumulation model for natural soft clays below railways

Hossein Tahershamsi [a,*], Reza Ahmadi Naghadeh [b], Bruno Zuada Coelho [c], Jelke Dijkstra [a]

[a] *Chalmers University of Technology, Department of Architecture and Civil Engineering, SE-41296 Gothenburg, Sweden*
[b] *Jönköping University, School of Engineering, SE-55111 Jönköping, Sweden*
[c] *Deltares, Department of Geo-engineering, 2600 MH Delft, the Netherlands*

ABSTRACT

An improved constitutive model for strain accumulation of natural clays under undrained cyclic loading is presented. The proposed model includes a formulation for the non-linear small-strain stiffness in the over-consolidated regime, along with a modified hardening law for cyclic accumulation to improve the tracking of strain accumulation at small stress amplitudes. To calibrate and validate the proposed model, a series of laboratory tests were conducted to study the cyclic response of natural Swedish clays, the effect of loading amplitude and pre-shearing history. Good agreement between predicted and measured accumulated axial strains and excess pore water pressures was obtained with different loading amplitudes. The findings reveal that the undrained pre-shearing has a substantial impact on the rate of accumulated strain, with pre-sheared samples exhibiting lower resistance values. The proposed and validated model opens up possibilities to study the monotonic and non-monotonic quasi-static response of soft clays below railway embankments over the lifetime of the structure, *i. e.* including the effects of construction, operation and decommissioning.

Introduction

In most developed countries with well-established and extensive railway networks the majority of expenses associated with the operation and maintenance of physical railway infrastructures are related to the maintenance of track geometry, which mainly addresses a Serviceability Limit State (SLS) problem [57,31]. The properties of subsoil govern the track modulus [41], and it remains one of the most persistent sources of degradation, as other components of the railway system, such as track, ballast and back-fill material, can be addressed cost-effectively during maintenance cycles. There are numerous studies into the degradation of ballast and other subgrade materials that are classified as coarse grained soils. These experimental studies investigate the volumetric compaction, rolling and particle breakage-driven degradation under various conditions of saturation and confinement pressure [19,47,8,56,5, *e.g.*]. In addition, the problem has been approached by means of numerical and empirical modelling [46,36,12,1,29,16, *e.g.*], as well as discrete element models [30,32,17, *e.g.*].

This study aims to investigate the cyclic degradation of natural soft clays beneath a railway embankment by capturing the interaction

between slow transient processes, such as consolidation, creep, and monotonic/non-monotonic quasi-static loading throughout the lifetime of the geostructure. The evolving pore water pressures significantly affect the response of the railway system [39], causing delayed settlements resulting from consolidation and creep [60]. Moreover, during the construction of the railway embankment, the deviatoric stress in the subsoil increases, affecting the natural clay's resilience for subsequent cyclic loading. The undrained cyclic loading results in excess pore water pressures and irreversible strains that accumulate over time [54]. Powrie et al. [37] have demonstrated that, due to the dispersion of the Raleigh wave in depth, only low frequencies are significant for an element of the soil below the embankment. Additionally, the inertial component of acceleration is considered low in case of small loading amplitudes [53]. Therefore, the degradation in the soft soil beneath the subgrade and the embankment is driven by non-monotonic quasi-static loading.

The cyclic response of natural clays is equally complex as that of more coarse-grained geomaterials, since it depends on loading rate and loading amplitude [58,2,27,51,54]. Another influential factor on the response is the order of application of load cycles, *i.e.* a complex loading

* Corresponding author.
E-mail addresses: hossein.tahershamsi@chalmers.se (H. Tahershamsi), reza.ahmadi@ju.se (R. Ahmadi Naghadeh), bruno.zuadacoelho@deltares.nl (B. Zuada Coelho), jelke.dijkstra@chalmers.se (J. Dijkstra).

Table 1

Index properties of Kärra clay. ρ_b bulk density; LL: Liquid Limit; PL: Plastic Limit; PI: Plastic Index; w_N natural water content; S_t sensitivity (fall cone).

Depth (m)	Unified symbol	ρ_b (g m^{-3})	LL (%)	PL (%)	PI (%)	w_N (%)	S_t (-)
9	CH	1.58	75.2	27.6	47.6	71.6	6.4

history [11]. Earlier studies have identified a critical stress ratio for soft clays under undrained cyclic loading [40,3, *e.g.*]. This critical stress level is associated with shakedown behaviour, where small amounts of plastic strain accumulate during repeated loading, leading to deformation due to cyclic creep. In the events of large loading amplitudes, the clay experiences ratcheting, a phenomenon in which the material accumulates additional plastic deformation with each loading cycle, eventually leading to failure due to excessive plastic strain. [38]. The most comprehensive design methodology with which to assess the cyclic response of foundations is centred on the Ultimate Limit State [2]. Conversely, the Serviceability Limit State (SLS) criteria, which are crucial for railway foundations on soft clays, are not considered. In particular, the high-fidelity prediction of strain accumulation, a key factor impacting SLS design, remains a challenge. Some empirical methods for strain accumulation have been proposed, but are unable to incorporate more complex stress histories as part of the analysis [26, *e.g.*]. A predictive model that not only predicts accumulated strains from cyclic loading, but also considers the complexities inherent in natural soft clays, such as anisotropy, destructuration and rate dependency, is essential [25,52,33,24].

Two separate predictive approaches have been developed to model the emerging strains from soils under cyclic loading [36]. In the implicit approach, the entire stress–strain behaviour is modelled as a function of time. The implicit approach for modelling soft soils most commonly employs models based on the bounding surface approach [34,28,49, *e.g.*]. In contrast, the explicit method, which is frequently utilised for a high number of loading cycles, explicitly prescribes the rate of strain accumulation resulting from cyclic loading [7,35,45,59]. The latter models are usually developed based on experimental tests with relatively high loading amplitudes.

This paper presents an improved strain accumulation model for natural soft clays, building upon the research of Zuada Coelho et al. [59]. The model enhances the ability to capture the low-amplitude cyclic loading paths that are characteristic of soil elements beneath railway embankments. The two major model improvements are (i) a simplified formulation for the cyclic hardening law inspired by Janbu [22] (ii) the inclusion of a smooth function for the small-strain stiffness in the elastic domain [43]. In addition, a new series of undrained cyclic triaxial tests were performed on a naturally sensitive clay from Sweden, for the purpose of validating the proposed new model. The tests include undrained pre-shearing and post-shearing for some of the specimens.

Experimental programme

The experimental tests have been performed on intact samples of Swedish natural clay from the Kärra test site in northern Gothenburg. The samples have been taken from 9m depth by using a Swedish STII sampler [42]. It should be noted that the clay is classified as slightly overconsolidated, with an OCR value of less than 2. The index properties of the clay are summarised in Table 1. The clay is characterised as highly plastic clay (CH) according to the Unified Soil Classification System [6]. The composition is determined as 71% clay sized particles with mainly illite mineral, 28% silt and the remainder larger fractions with a grain size larger than 50μm.

At the site, the water table is close to the ground surface. Hence, the *in situ* stress state at the depth of the samples taken corresponds to a mean effective stress p_0' of 52kPa and a deviatoric stress q_0 of 28kPa. The average shear modulus, measured with a seismic dilatometer at a comparable depth in sites nearby with similar geological deposition history, is $G_{max} = 17.5 \pm 2.5$MPa [55].

Test setup

A conventional computer-controlled Bishop and Wesley [4] type of hydraulic stress path apparatus, equipped with a submersible internal load cell, was modified to perform cyclic loading tests on 50mm diameter specimens that are 100mm tall. Preliminary tests were conducted using two submersible displacement transducers mounted to the mid-section of the sample to measure axial strains in the soft clays [10]. These tests confirmed that the use of external transducers with which to measure axial strains was sufficiently accurate, given the slightly low stiffness of the samples, as indicated by comparison with the complementary local instrumentation. Hence, for the purpose of this paper, all experimental data are considered of similar quality.

To capture the changes in pore water pressures during undrained monotonic shearing and subsequent undrained cyclic loading stage, a cyclic load was applied with a sufficiently low loading rate (a sinusoidal load with period T of 180s) as per the limitations of testing apparatus. Pore water pressures were measured at the base of the sample. A suction cap was employed to enable the performance of cyclic loading towards the extension regime and to centre the applied load between the load cell and top plate. Paper side drains were used to speed up the consolidation stage. The cell fluid was Paraffin oil, whereas the back pressure lines were saturated with tap water. In the presented test series GDS instruments controllers were used to control cell, back and ram pressure during the consolidation, undrained pre-shearing and cyclic loading stages.

Experimental procedure

A total of eight carefully planned cyclic undrained triaxial tests were performed on high-quality cylindrical undisturbed natural clays samples taken from 9m depth. However, Test 10 had to be excluded from this paper because of significant fluctuations in the readings that occurred

Table 2

Summary of undrained cyclic triaxial tests for Kärra clay.

Test	Duration	Stages[1]	p_0'	q_0	q_p	q_m	q_{cyc}	$\frac{q_{cyc}}{p_0'}$	Cyclic failure
-	day, d		kPa	kPa	kPa	kPa	kPa	-	-
4	16.98	I, J, K, L, M, N	53.83	28.00	19.00	47.00	5	0.09	No
5	36.84	I, J, M, N	49.53	28.00	0.00	28.00	5	0.10	No
6	58.81	I, J, M, N	51.03	29.80	0.00	29.80	10	0.20	No
7	108.90	I, J, M	55.70	29.10	0.00	29.10	20	0.36	Yes
8	19.10	I, J, K, L, M	53.10	28.50	9.00	37.70	20	0.38	Yes
9	14.07	I, J, M	52.63	28.30	0.00	28.30	28	0.53	Yes
11	20.08	I, J, K, L, M	49.60	27.90	−8.00	20.30	38	0.77	Yes

[1] I = anisotropic consolidation, J = saturation, K = pre–shearing, L = creep, M = cyclic loading, N = post-cyclic monotonic shearing
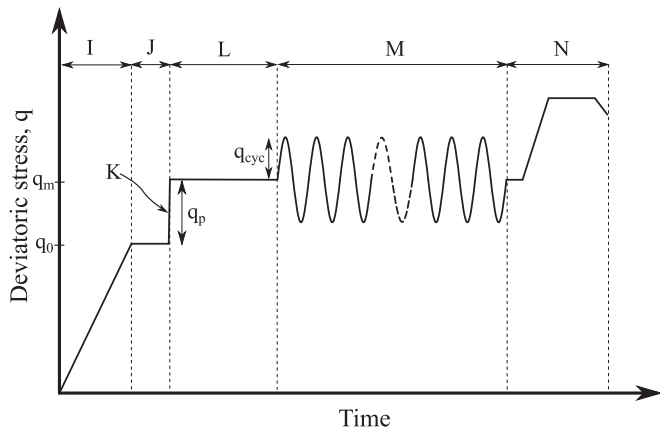
Fig. 1. Definition of stages: I – anisotropic consolidation; J – saturation; K– pre–shearing; L – creep; M – cyclic loading; N – post-cyclic monotonic shearing. Stages K to N have been performed under undrained conditions.

Fig. 2. The overview of undrained cyclic triaxial tests in $q_m - q_{cyc}$ space. The reported initial stresses are measured at the end of the anisotropic consolidation stage.

due to external interruptions during the test. The specification of the cyclic undrained triaxial tests, with the exception of Test 10, is summarised in Table 2. The duration of the pore water equalisation stage at the end of consolidation was substantially longer (multiple days) to help discern (deviatoric) creep under constant load from the accumulated strain under cyclic loading. This explains the somewhat large variation in p'_0 and q_0 achieved after the consolidation stage, listed in Table 2. After assessing the monotonic results of the anisotropically-consolidated undrained compression test (CAUC), only samples from 9m depth were used for the cyclic tests. The systematic testing of samples from a single depth enables isolating the impact of pre-shearing and loading amplitude on the results and simplifies the calibration procedure. As such, the complete tests were stress controlled, whereas the emerging (accumulated) strains and (excess) pore water pressures were measured during the test.

The experimental loading procedure involved several loading components, as shown in Fig. 1. The stages are summarised as follows:

1. Stage I: During the first stage of the experimentation, the samples underwent an anisotropic consolidation phase by imposing the deviatoric stress q_0, which was meant to simulate the *in situ* conditions.
2. Stage J: A stage dedicated to equalising the pore water pressures was conducted after the consolidation stage has been completed.
3. Stages K & L: In some of the tests, such as Tests 04, 08, 11, an undrained pre-shearing stage K was included, and the magnitude of q_p was adjusted accordingly. To maintain undrained conditions during the tests, the back pressure line was closed after the completion of consolidation. Moreover, a subsequent creep stage L was conducted after the loading/unloading stage in these tests.
4. Stage M: Subsequently, the resulting superimposed deviatoric stress q_m ($q_m = q_0 + q_p$), was subjected to an undrained cyclic loading with amplitude q_{cyc}. To avoid exceeding the critical limit for maximum stress, the value of q_{cyc} was chosen such that the combined deviatoric stress ($q_m + q_{cyc}$) did not exceed twice the undrained shear strength ($q_{max} = 2s_u$). The undrained shear strength was determined from the monotonic tests as $s_u = 33$kPa.
5. Stage N: Tests 04, 05 and 06, which were not failed during the cyclic loading stage at low amplitudes, were eventually sheared monotonically to failure under undrained conditions.
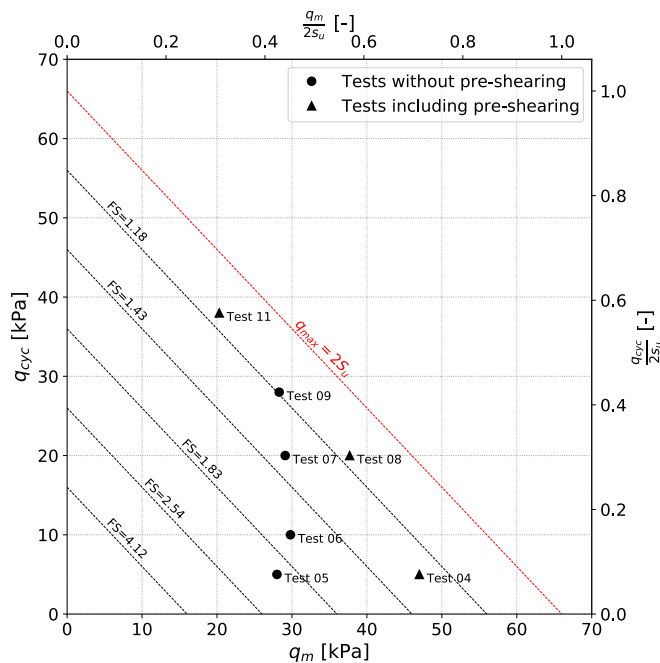
A general overview of the loading programme in q_m - q_{cyc} space is shown in Fig. 2. The red diagonal (drawn at a -45° angles) represents the critical limit for maximum stress q_{max}. Based on q_{max}, subsequent diagonal lines are calculated with the intervals of 10kPa. Thus, the Factor of Safety (FS) on each diagonal line is defined as the ratio of the ultimate deviatoric stress q_{max} to the corresponding allowable deviatoric stresses. An average test duration of 38 days is required to first consolidate the samples anisotropically, and subsequently apply a minimum of 10 000 load cycles (in case the sample does not fail prematurely). Some tests, such as Test 07, were allowed to continue up to 45 000 loading cycles (total test duration of 3 months), whereas other tests (*i.e.* Tests 04, 05, 06) were aborted prematurely, and subsequently sheared to failure in undrained conditions.

Note that two series of tests can be identified: in the first series, the mean stress q_m is kept constant and the impact of cyclic loading amplitude q_{cyc} will be studied (Tests 05, 06, 07 & 09). In the second series with pre-shearing, the q_m is increased or reduced in an undrained loading step while changing q_{cyc} to preserve a comparable FS compared to the test that is anisotropically consolidated into *in situ* conditions (Tests 04, 08 & 11). The main motivation for this loading protocol is to isolate the impact of loading amplitude from the effect of pre-loading resulting from such factors as embankment construction (loading) and or an excavation (unloading). The tests without pre-shearing will be used for revising the hardening law in the model. The data with pre-shearing will be used to validate the constitutive model for more complex loading histories.

Cyclic creep

Given the difficulty in separating the effects of creep and cyclic loading from the raw data, numerical simulations with the Creep-SCLAY1Sc model has been used to identify the need for the strain accumulation model for small loading amplitudes. Appendix A provides a brief overview of the Creep-SCLAY1Sc model parameters. The model is implemented at the boundary value level in the Tochnog Professional Finite Element code used for simulating an axisymmetric sample of 25mm radius and 100mm height, using a single 4 noded element. The displacements on the symmetry axis and bottom are fixed, whereas the external loads on the other boundaries control the confinement and axial stress following the experimental protocol. Furthermore, a coupled hydro-mechanical formulation using the storage equation (using a hydraulic conductivity of 8.64×10^{-5}m d^{-1}) was used to model the
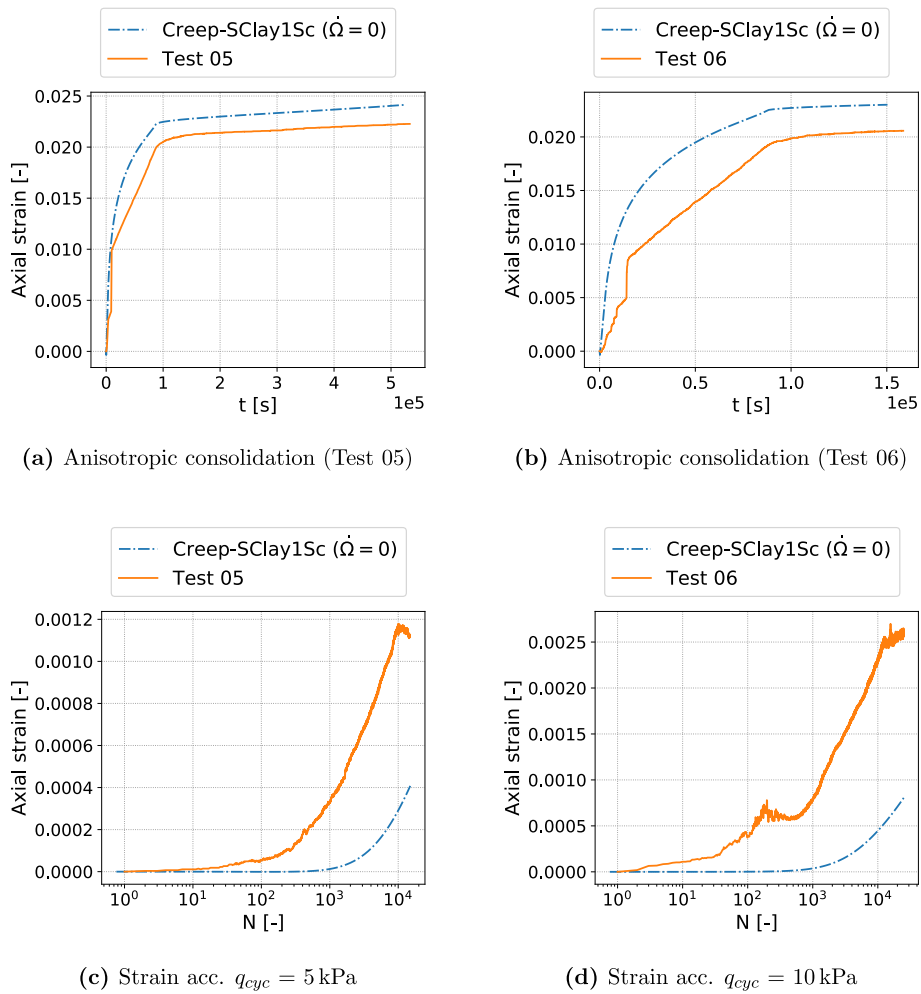
(a) Anisotropic consolidation (Test 05)

(b) Anisotropic consolidation (Test 06)

(c) Strain acc. $q_{cyc} = 5\,\text{kPa}$

(d) Strain acc. $q_{cyc} = 10\,\text{kPa}$

Fig. 3. Comparison of Creep-SCLAY1Sc with experimental data for irreversible axial strains.

(a) Strain acc. $q_{cyc} = 5\,\text{kPa}$

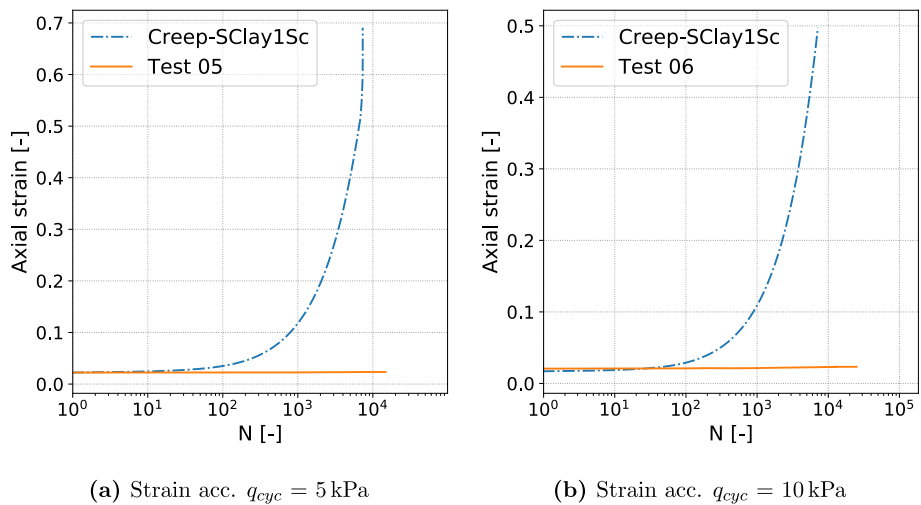**(b)** Strain acc. $q_{cyc} = 10\,\text{kPa}$

Fig. 4. Comparison of Creep-SCLAY1Sc model with experimental data during undrained cyclic loading.

generation and dissipation of excess pore water pressures during all stages of the test.

The experimental results of the two tests with low loading amplitudes (*i.e.* Test 05 & 06) are compared to the predictions by the Creep-SCLAY1Sc model in which the cyclic accumulation component $\dot{\Omega}$ in Eq. 27 is suppressed to zero; thus, in the model the strain is accumulated

due to creep alone [44,14]. In Figs. 3a and 3b, the model prediction is compared to the experimental stage for consolidation and creep, prior to the cyclic loading of Tests 05 and 06, demonstrating the ability of the model to capture the creep rates. Fig. 3c and 3d indicate that for small loading amplitudes, the measured accumulated strain due to cyclic loading is larger than the anticipated axial strain from deviatoric creep

only.

Subsequently, the Creep-SCLAY1Sc model is calibrated against the experimental data, with the model parameters reported in Section 3.2. In this step, the cyclic accumulation multiplier $\dot{\Omega}$ is invoked in the formulation as Eq. 27, in order to model the cyclic loading stage of Tests 05 & 06. By comparing the numerical results against the data in Fig. 4, however, the results obtained are poor. The predicted axial strains overestimate the test results by a large margin, and furthermore a failure mechanism is predicted by the model. The magnitudes of irreversible axial strain during the experiments are an order of magnitude smaller than predicted by the model and in the experimental results no failure is observed. For small loading amplitudes q_{cyc}, the cyclic accumulation multiplier $\dot{\Omega}$ in Eq. 28, is overestimated. Therefore, in its current formulation, Creep-SCLAY1Sc, developed on data with large loading amplitude, appears not to be suitable for the prediction of cyclic strain accumulation for small loading amplitudes, despite its amplitude dependency. Thus, the model formulations needs some revision.

Revised cyclic accumulation model

The cyclic accumulation model presented herein is a revision of the Creep-SCLAY1Sc model originally proposed by Zuada Coelho et al. [59], exploiting the resistance concept of Janbu [20] and new data from a Swedish high plasticity natural clay. By using the resistance concept, an assumption is made that the small loading amplitudes and low loading frequencies, as observed in the soft clays below railway infrastructure, are reflected by a viscoplastic response that is a function of the degree of overconsolidation. Hence, the main changes are in the hardening law for the accumulation of strains during cyclic loading. Furthermore, features that capture the stiffness response at small strain (loading amplitudes) are added. As an advantage, the proposed modification simplifies the derivation of model parameters from undrained cyclic triaxial tests.

Janbu's resistance concept

Janbu [20] introduced the resistance concept for the deformation of soils. The resistance of a medium, or a control volume thereof, is defined as:

$$R = \frac{\text{differential cause}}{\text{differential effect}} \tag{1}$$

For a given soil under cyclic loading with a constant deviatoric stress amplitude, strain resistance is written as:

$$R_\epsilon = \frac{dN}{d\epsilon} \tag{2}$$

In Eq. 2, R_ϵ is strain resistance, N is the number of loading cycles, and ϵ is the accumulated irreversible strain. In most experiments on (slightly) overconsolidated clays, R_ϵ increases nearly linearly N until the onset of failure [21,22], therefore:

$$R_\epsilon = m_\epsilon N \tag{3}$$

In Eq. 3, m_ϵ is a dimensionless resistance number for strain accumulation. By rearranging Eqs. 2,3 and solving the differential equation over $[1 \sim N]$, the change in the (viscoplastic) volumetric strain is found as a function of the number of loading cycles N:

$$\Delta \epsilon_v^{vp} = \frac{1}{m_\epsilon} \ln N \tag{4}$$

The isotropic component of the hardening rule of the (anisotropic) viscoplastic Creep-SCLAY1S model is provided in Eq. 5 [14]:

$$\frac{dp_p'}{d\epsilon_v^{vp}} = \frac{p_p'}{\zeta_i^*} \qquad \text{where} \quad \zeta_i^* = \lambda_i^* - \kappa^* \tag{5}$$

in which, ζ_i^* is an intrinsic parameter related to irrecoverable compression, κ^* is the modified swelling index and λ_i^* is the modified intrinsic compression index. The integration of Eq. 5 over equivalent mean effective stress p_{eq}' to the stress that corresponds to the projected mean effective preconsolidation pressure p_p', yields:

$$\Delta \epsilon_v^{vp} = \zeta_i^* \ln \left(\frac{p_p'}{p_{eq}'} \right) \tag{6}$$

Eq. 7 is obtained by equating Eqs. 2,.

$$\frac{dN}{d\epsilon} = m_\epsilon N \tag{7}$$

The combination of Eqs. 4,6,7, where time is introduced as $t = NT$ for the cyclic loading with constant loading period T, results in:

$$\frac{d\epsilon_v^{vp}}{dt} = \frac{1}{m_\epsilon T} \left(\frac{p_{eq}'}{p_p'} \right)^{m_\epsilon \zeta_i^*} \tag{8}$$

Cyclic accumulation formulation

The proposed constitutive model uses a similar strain decomposition as the original Creep-SCLAY1Sc model:

$$\dot{\epsilon}_{ij} = \dot{\epsilon}_{ij}^e + \underbrace{\left(\dot{\epsilon}_{ij}^c + \dot{\epsilon}_{ij}^{cyc} \right)}_{\dot{\epsilon}_{ij}^{vp}} \tag{9}$$

where in Eq. 9, $\dot{\epsilon}_{ij}^e$ is the tensor of elastic strain rate, $\dot{\epsilon}_{ij}^{vp}$ viscoplastic strain rate, $\dot{\epsilon}_{ij}^c$ creep strain rate, and $\dot{\epsilon}_{ij}^{cyc}$ the cyclic strain rate. An additional viscoplastic multiplier $\dot{\Gamma}$ that captures the cyclic accumulation is added to the original creep viscoplastic multiplier. Thus, $\dot{\epsilon}_{ij}^{vp}$ becomes:

$$\dot{\epsilon}_{ij}^{vp} = \left[\dot{\Lambda} + \dot{\Gamma} \right] \frac{\partial p_{eq}'}{\partial \sigma_{ij}'} \tag{10}$$

Eq. 10 implies that the viscoplastic strain resulting from the cyclic loading follows the same direction as the viscoplastic creep strain. Therefore, the associated flow rule is maintained.

The viscoplastic multiplier for creep $\dot{\Lambda}$ can be written in terms of Janbu's resistance concept as [15]:

$$\dot{\Lambda} = \frac{1}{r_{si}\tau} \left(\frac{p_{eq}'}{p_p'} \right)^{r_{si}\zeta_i^*} \left(\frac{M(\theta)^2 - \alpha_{K_0^{nc}}^2}{M(\theta)^2 - \eta_{K_0^{nc}}^2} \right) \tag{11}$$

In Eq. 11, r_{si} is the intrinsic time resistance number, with reference time τ. M, the stress ratio at critical state, is a function of the modified Lode angle θ. $\alpha_{K_0^{nc}}$ is the inclination of surfaces in the normally consolidated state and $\eta_{K_0^{nc}}$ corresponds to the stress ratio for a clay in its normally consolidated state; K_0^{nc} [14].

Following Eq. 8, the viscoplastic multiplier for cyclic accumulation $\dot{\Gamma}$ is defined as:

$$\dot{\Gamma} = \frac{1}{|m_\epsilon| T} \left(\frac{p_{eq}'}{p_p'} \right)^{\psi \zeta_i^*} \tag{12}$$

where ψ is a scaling parameter that scales the impact of 'overconsolidation ratio' on the magnitude of the cyclic strain accumulation. When compared to Eq. 8, ψ replaces m_ϵ in the exponent to prevent overly attenuated viscoplastic strains at large values for m_ϵ that correspond to low cyclic loading amplitudes q_{cyc}.
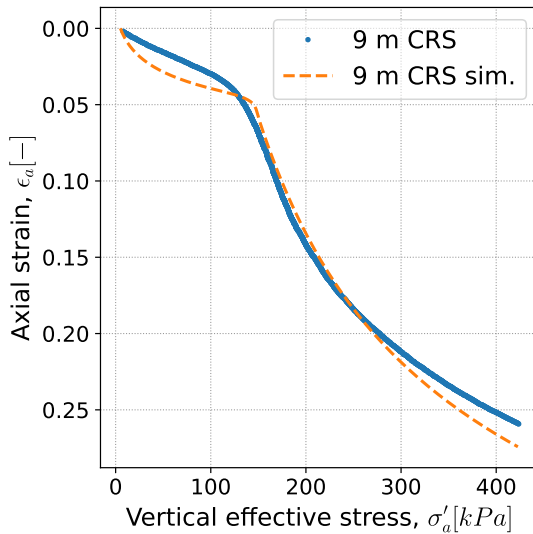
Fig. 5. Comparison of model calibration with the results of a CRS test at a depth of 9m.

Small strain stiffness formulation

Conventional lab tests, such as triaxial or oedometer tests, typically yield a soil stiffness that is lower than its initial value at levels of small strains. In sensitive clays that are slightly overconsolidated, Wood [55] has observed a decrease in stiffness as the magnitude of strain increases. Since soil stiffness varies across levels of minor strains, incorporating small-strain soil stiffness and its nonlinear dependency results in a more reliable interpretation of both laboratory tests and field measurements [23].

As part of the implementation of the cyclic accumulation relations into Creep-SCLAY1S, the elastic stiffness matrix D_{ijhk} that is dependent on the mean effective stress p', needs to be assembled. A 6×6 stiffness matrix according to Hooke's law is assembled, where the volumetric elastic compression in the overconsolidated region κ^* and the Poisson ratio ν from Creep-SCLAY1S, are used to calculate the shear modulus G as Eq. 13:

$$G = \frac{3p'(1 - 2\nu)}{2\kappa^*(1 + \nu)} \tag{13}$$

Subsequently, the components of D_{ijhk} are calculated as Eq. 14, in which the index notation of δ represents the Kronecker delta.

$$D_{ijhk} = \frac{2G\nu}{1 - 2\nu}\delta_{ij}\delta_{hk} + G\left(\delta_{ik}\delta_{jh} + \delta_{ih}\delta_{jk}\right) \tag{14}$$

The small-strain extension simply replaces G with an expression that depends on the strain history, and the highest attainable stiffness at small strain G_{max}. There are many options [18,9, *e.g.*], however, in this study a suggestion by Sivasithamparam et al. [43] is followed, *i.e.*:

$$G = G_{max}\left[1 - \frac{\langle\varepsilon_q - \varepsilon_s\rangle}{A + B\langle\varepsilon_q - \varepsilon_s\rangle}\right] \tag{15}$$

where G_{max} is the reference stiffness at small strain, which remains a function of the mean effective stress p'. In Eq. 16, the multiplier ϖ relates the shear modulus in the overconsolidated regime as determined in normal laboratory tests at engineering strain levels as G_{max}. The maximum shear modulus G_{max} will be reduced towards a limiting value that is controlled by parameters A and B and the shear strain history. The deviatoric component of the total shear strain ε_q is compared to a threshold value ε_s, which is set internally at 10^{-5}. The symbols $\langle \bullet \rangle$ are Macaulay brackets that return $(\varepsilon_q - \varepsilon_s)$ for $(\varepsilon_q - \varepsilon_s) > 0$ and 0 otherwise.

$$\kappa_0^* = \frac{\kappa^*}{\varpi} \tag{16}$$

It would be logical to choose values for A and B, such that G ranges between G_{max} and G_{ur} at engineering strain levels. G_{ur} denotes the unload/reload shear modulus (*i.e.* the stiffness in the overconsolidated range). By rearranging Eq. 15, the true limit when $\langle\varepsilon_q - \varepsilon_s\rangle \rightarrow \infty$ becomes:

$$\lim_{\langle\varepsilon_q - \varepsilon_s\rangle \rightarrow \infty}\left[1 - \frac{\langle\varepsilon_q - \varepsilon_s\rangle}{A + B\langle\varepsilon_q - \varepsilon_s\rangle}\right] = 1 - \frac{1}{B} \tag{17}$$

Thus, the model parameter B sets the span in attainable stiffness between G_{ur} and the small strain stiffness G_{max}; see Eq. 18.

$$B = \frac{1}{1 - \frac{G_{ur}}{G_{max}}} \tag{18}$$

Model calibration

The model components carried over from the original model, inherited from the Creep-SCLAY1S model, include the 14 model parameters that correspond to features such as isotropic hardening, rotational hardening, degradation of bonds and rate-dependency [44,14]. These model parameters are derived from a set of incremental loading oedometer tests, as well as anisotropically consolidated triaxial tests that are sheared in compression and extension.

Five additional parameters are introduced in the current paper to capture the amplitude dependent cyclic accumulation and small strain stiffness in soft natural clays. Based on the theory presented in Sections 3.1 and 3.2, three parameters (*i.e.* T, m_ϵ, and ψ) are introduced in order to capture the accumulation of strain due to cyclic loads with a constant loading period. Two additional model parameters (*i.e.* A and ϖ) are included to model the non-linear elasticity. The resulting secant shear modulus ranges from G_{max} at small strain and G_{ur} as a function of the total deviatoric strain in the overconsolidated region of the model, following the empirical relation in Eq. 15.

Monotonic parameters

The model parameters for the features that capture the monotonic quasi-static rate-dependent behaviour of the natural clay are initially calibrated against the experimental results from Kärra clay. The base-model Creep-SCLAY1S serves as the source of monotonic parameters, some of which cannot be directly measured [13]. Anisotropy parameters $(\alpha_0, \omega, \omega_d)$ and parameters related to destructuration (χ_0, a, b) require manual fitting to experimental data or follow recommendations by Gras et al. [14]. The evaluation procedure for all model parameters is as follows:

- The values of κ^*, λ_i^*, and σ'_{p_0} were derived from the Incremental Loading (IL) and Constant Rate of Strain (CRS) oedometer data, on samples taken from 9m depth. κ^* and λ_i^* respectively represent the elastic and intrinsic slope of the $\ln\sigma'_v - \varepsilon$ curve, where σ'_v denotes the vertical effective stress. The pre-consolidation pressure σ'_{p_0} evaluated by the CRS test following the approach in Sällfors [48]. Fig. 5 shows the verification of the simulation at the element level with the experimental result of the CRS test.
- The intrinsic time resistance number r_{si}, is determined from the time series of the IL oedometer test corresponding to a load step at very large stress levels where all initial fabric has been remoulded. r_{si} is obtained by calculating the natural logarithm of the ratio of two time intervals $(\Delta\ln(t))$ and dividing it by the change in strain over the same time intervals $(\Delta\varepsilon)$ during the secondary consolidation.
- The slopes of the Critical State Line (CSL) in compression and extension are represented by M_c and M_e, respectively. Fig. 6 displays
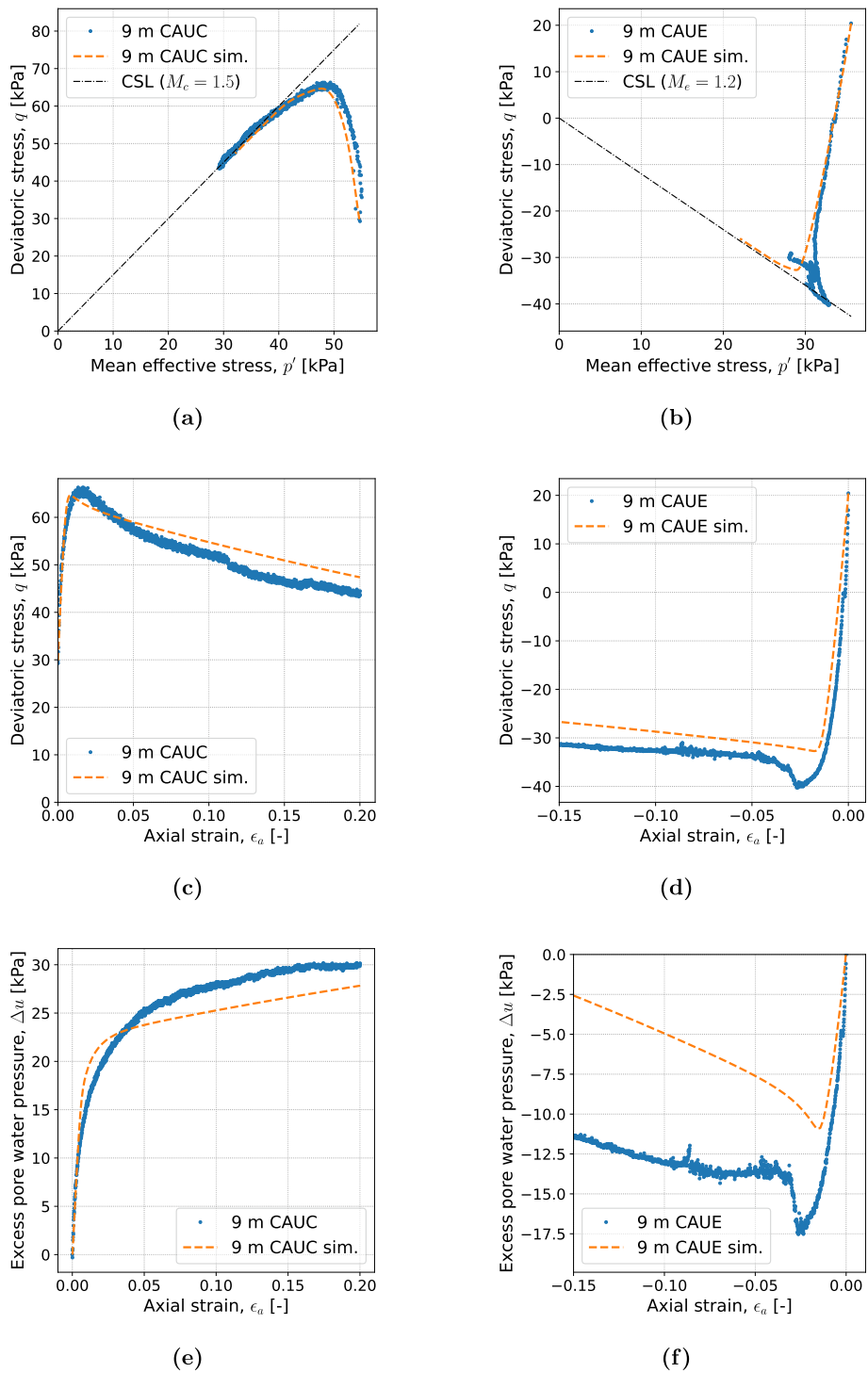
Fig. 6. Model calibration for CAUC, CAUE tests taken from 9m depth.

the results of simulations for the Anisotropically Consolidated Undrained test in Compression (CAUC) and Extension (CAUE). In the CAUC test, the stress path tends to approach the CSL with a stress ratio of $M_c = 1.5$, as illustrated in Fig. 6a. Similarly, the stress path of the CAUE test tends to approach the CSL with a stress ratio of $M_e = 1.2$, as depicted in Fig. 6b. The stress–strain relation and excess pore water pressure values obtained from the CAUE simulation were found to be conservative, as evidenced by the simulations presented in Figs. 6d and 6f. Conversely, the undrained compression test exhibited a higher degree of agreement, as shown in Figs. 6c and 6e.

- The model parameter ω, which controls the rate and development of anisotropy, was calibrated through the CAUE test. To calculate the remaining anisotropic parameters, such as α_0 and ω_d, empirical relations proposed by Gras et al. [14] are used, as they cannot be determined experimentally. Specifically, Eqs. 19 and 20, are utilised to determine α_0 and ω_d, respectively.

$$\alpha_0 = \frac{\eta_{K_0^{nc}}^2 + 3\eta_{K_0^{nc}} - M_c^2}{3} \tag{19}$$

Table 3

Monotonic model parameters for Kärra clay.

Parameter	Description	Unit	Value
κ^*	Modified swelling index	-	0.0166
ν'	Poisson's ratio	-	0.2
λ_i^*	Modified intrinsic compression index	-	0.0824
M_c	Slope of CSL in triaxial compression	-	1.5
M_e	Slope of CSL in triaxial extension	-	1.2
σ'_{p_0}	Initial effective preconsolidation pressure	kPa	110
α_0	Initial inclination of NCS	-	0.58
ω	Absolute effectiveness of rotational hardening	-	800
ω_d	Relative effectiveness of rotational hardening	-	1.0
χ_0	Initial amount of bonding	-	20
a	Absolute rate of destructuration	-	11
b	Relative rate of destructuration	-	0.15
r_{si}	Intrinsic time resistance number	-	182
τ	Reference time	d	1

$$\omega_d = \frac{3\left(4M_c^2 - 4\eta_{K_0^{nc}}^2 - 3\eta_{K_0^{nc}}\right)}{8\left(\eta_{K_0^{nc}}^2 - M_c^2 + 2\eta_{K_0^{nc}}\right)} \tag{20}$$

In Eqs. 19,20, $\eta_{K_0^{nc}}$ is defined as shown in Eq. 21. K_0^{nc} is obtained from Jaky's formula, and M_c is related to the internal friction angle through the expression $6\sin\phi'/(3-\sin\phi')$.

$$\eta_{K_0^{nc}} = \frac{3\left(1-K_0^{nc}\right)}{1+2K_0^{nc}} \tag{21}$$

The undrained triaxial extension test allowed for calibrating model parameter ω, controlling the rate of evolution of anisotropy.

- The destructuration parameter χ_0 indicates the initial amount of bonding in the natural clay, while parameters a and b control the rate of destructuration that leads to bond degradation [24]. The destructuration law is fitted using the element level simulation of the CRS test to demonstrate the model's ability to capture the clay response.

Table 3 presents the description of the monotonic model parameters and their corresponding values calibrated at element level. The model generally provides an accurate prediction of the stress–strain behaviour of Kärra clay under undrained deviatoric loading in compression and CRS loading path. However, the identification of a unique set of parameters that can effectively capture all pertinent stress paths poses a significant challenge, especially in the context of advanced constitutive models incorporating different model features [13,50].

Cyclic parameters

The parameters corresponding to the revised cyclic accumulation model are determined using the resistance concept described in Section 3.1. The strain resistances R_ϵ corresponding to the mean axial strain is determined from the data from the undrained cyclic triaxial tests, using
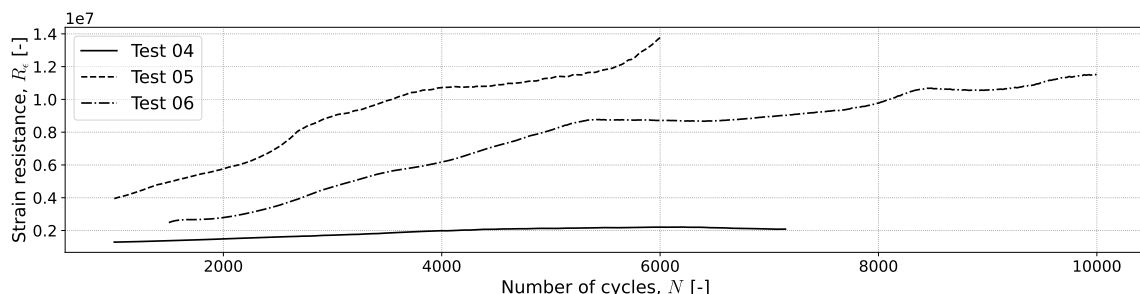
Eq. 2. Fig. 7 presents the strain resistance R_ϵ versus the number of cycles N for the tests without cyclic failure. A nearly linear relationship between the strain resistance and the number of cycles is observed, in line with the observations reported by Janbu [21]. However, the strain resistance reaches zero for samples at larger stress amplitudes towards the onset of failure. Thus, the absolute values of the resistance numbers, m_ϵ, are tabulated in Table 4. The values of m_ϵ range from 108 to 1808.

Table 4

Strain resistance numbers for Kärra experiments.

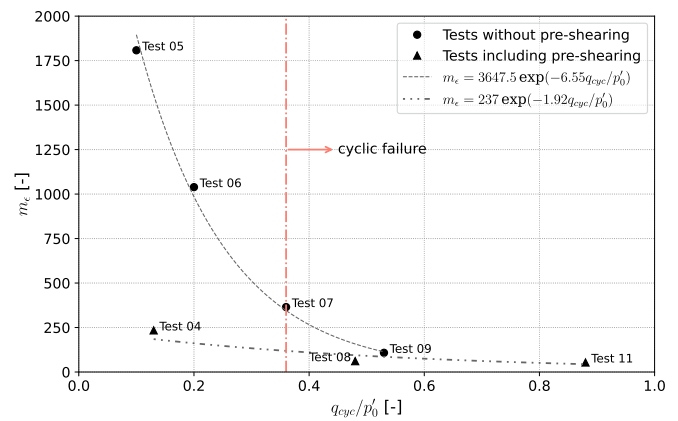| Test#	$|m_\epsilon|$	m_ϵ^*
Test 04	234	185
Test 05	1808	1883
Test 06	1039	1011
Test 08	61	95
Test 09	108	112
Test 11	54	44

Fig. 8. Relationship between the degree of shear mobilisation q_{cyc}/p_0' and the resistance number m_ϵ for Kärra samples.

Table 5

Evaluated ψ for samples with different degrees of shear mobilisation.

Shear mobilisation (q_{cyc}/p_0')	ψ
0–0.2	161
0.36–1.0	128

Table 6

Model parameters for small strain stiffness.

Parameter	Description	Unit	Value
ϖ	Small strain multiplier	-	8
A	Shape factor for small strain stiffness	-	5×10^{-3}

Fig. 7. Strain resistance for Tests 04, 05 and 06.

(a) Test 08; $q_{\mathrm{cyc}} = 20\,\mathrm{kPa}$ **(b)** Test 09; $q_{\mathrm{cyc}} = 28\,\mathrm{kPa}$ **(c)** Test 11; $q_{\mathrm{cyc}} = 38\,\mathrm{kPa}$
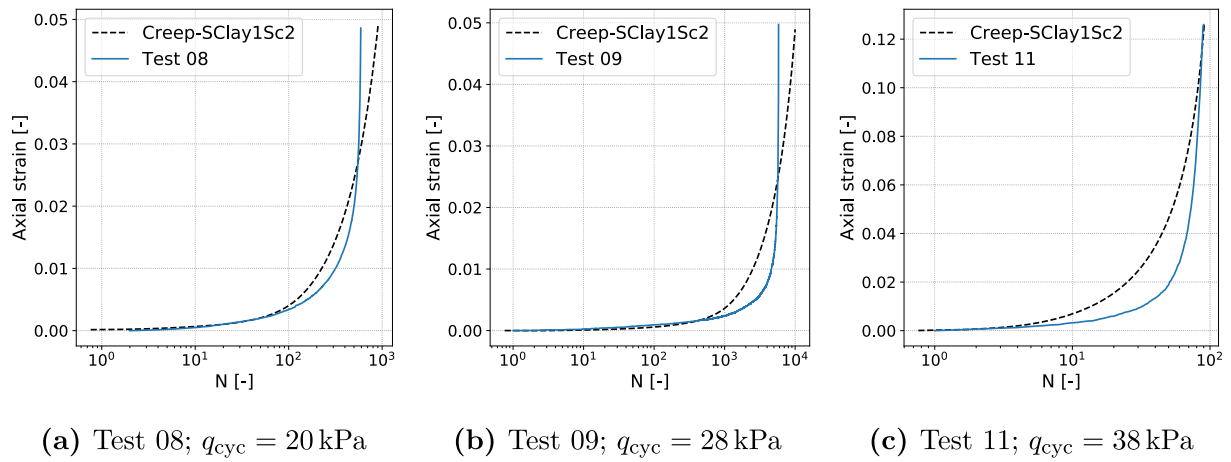
Fig. 9. Sample with relatively large loading amplitudes.

(a) Test 08; $q_{\mathrm{cyc}} = 20\,\mathrm{kPa}$ **(b)** Test 09; $q_{\mathrm{cyc}} = 28\,\mathrm{kPa}$ **(c)** Test 11; $q_{\mathrm{cyc}} = 38\,\mathrm{kPa}$
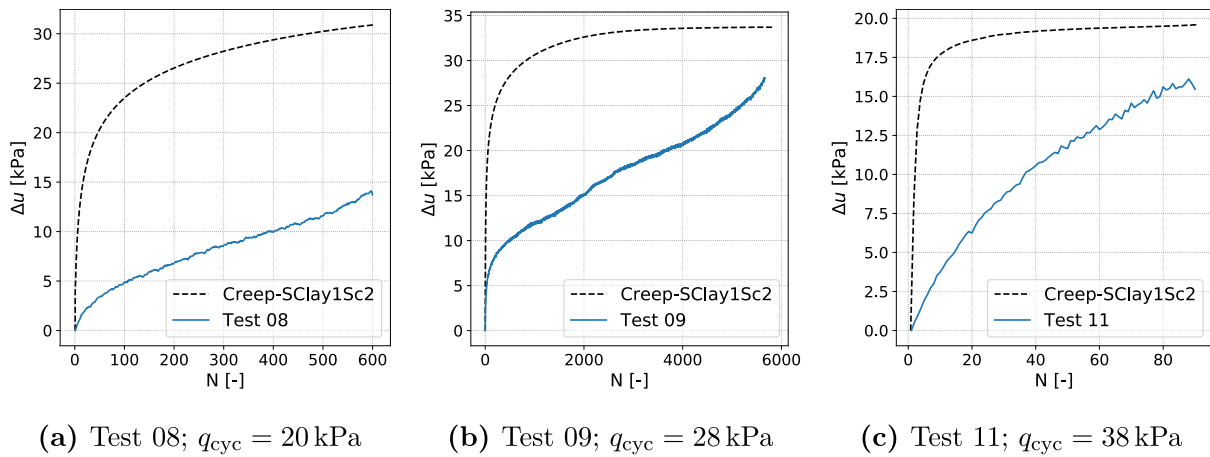
Fig. 10. Excess pore water pressures for samples with relatively large loading amplitudes.

(a) Test 04; $q_{\mathrm{cyc}} = 5\,\mathrm{kPa}$ **(b)** Test 05; $q_{\mathrm{cyc}} = 5\,\mathrm{kPa}$ **(c)** Test 06; $q_{\mathrm{cyc}} = 10\,\mathrm{kPa}$
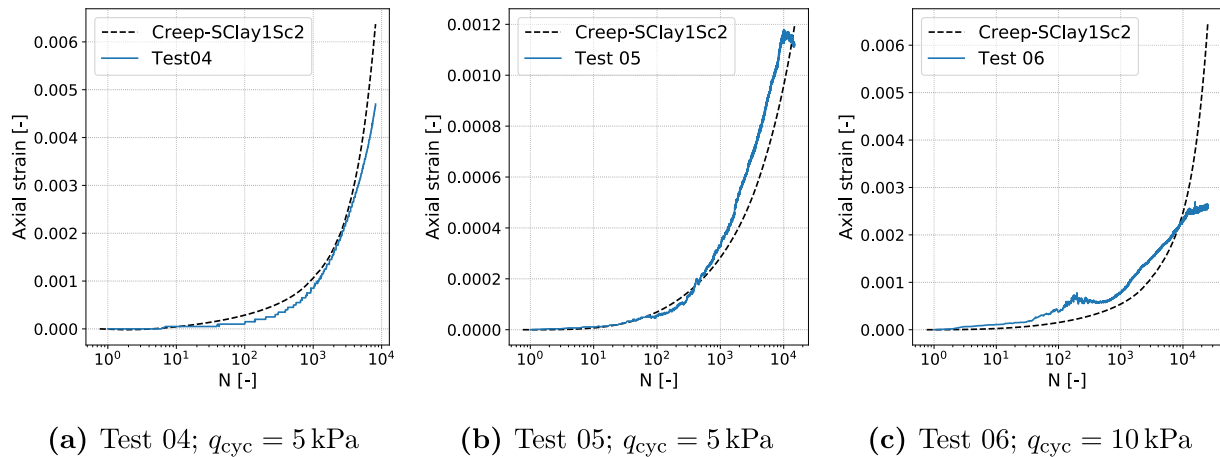
Fig. 11. Samples with relatively small loading amplitudes.

Tests 05 and 06 exhibit higher values of m_ϵ due to their low loading amplitudes and the absence of a pre-shearing stage.

By comparing the strain response in Fig. 7, Test 04 shows a lower resistance compared to Test 05 and Test 06 due to the pre-shearing stage prior to the application of cyclic loads. Clearly, the application of (un-drained) pre-shearing has a large impact on the subsequent cyclic response.

Additionally, the degree of mobilisation also influences the value of m_ϵ. Fig. 8 depicts the variation of m_ϵ for Kärra samples with respect to the applied shear stress amplitude q_{cyc}, normalised by the initial mean effective stress at the start of the cyclic loading stage p'_0. A vertical red line separates the tests that did not fail during cyclic loading from those that reached failure during the cyclic loading stage. In addition, the samples are categorised into two batches: tests including undrained pre-
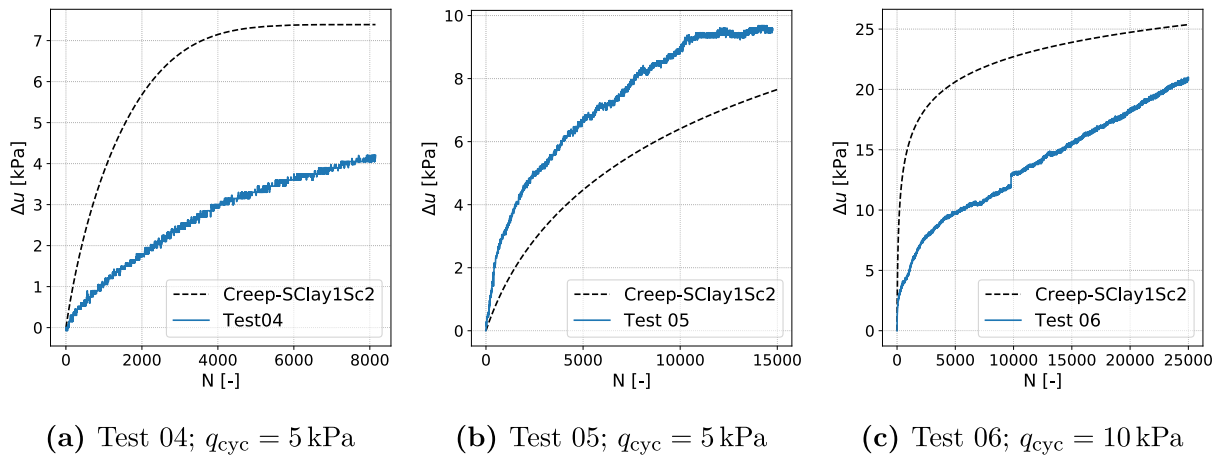
(a) Test 04; $q_{\mathrm{cyc}} = 5\,\mathrm{kPa}$ **(b)** Test 05; $q_{\mathrm{cyc}} = 5\,\mathrm{kPa}$ **(c)** Test 06; $q_{\mathrm{cyc}} = 10\,\mathrm{kPa}$

Fig. 12. Excess pore water pressure for samples with relatively small loading amplitudes.
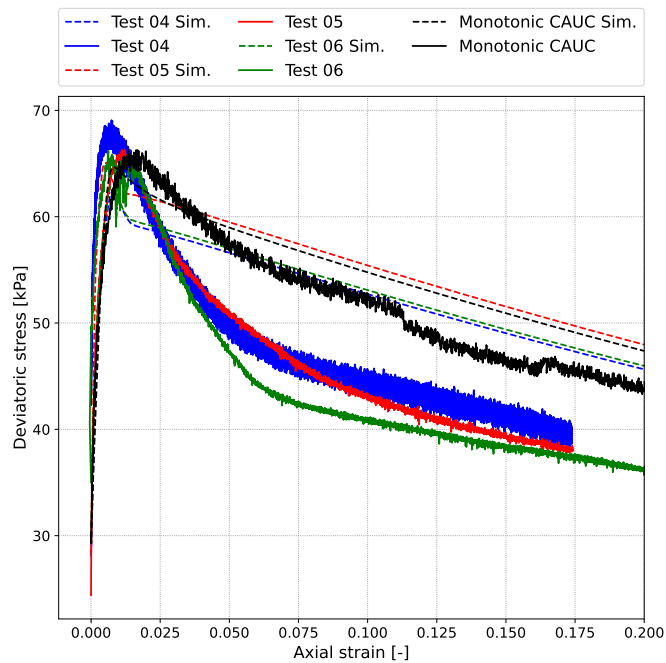
Fig. 13. Comparison of simulated and measured post-cyclic shearing stages with CAUC reference test.

Fig. 14. Creep-SCLAY1Sc and its associated surfaces [59].

shearing stages before the application of cyclic loading, and experiments without any pre-shearing, respectively. The experiments that underwent pre-shearing stages have significantly lower m_ϵ values compared to those without pre-shearing, indicating a decrease in resistance due to the disturbance caused by pre-loading prior to cyclic loading. The samples without cyclic failure (*i.e.* Test 04, Test 05, Test 06) feature higher m_ϵ than the tests with pre-shearing, as well as a lower stress ratio q_{cyc}/p_0' (because there is no reduction in effective stress prior to cyclic loading). An exponential relationship between m_ϵ and q_{cyc}/p_0' is found for the Kärra experiments shown in Fig. 8. Subsequently, a modified resistance number denoted as m_ϵ^* is evaluated for these tests based on the exponential relations, and the resulting values are presented in Table 4.

Based on the cyclic experiments performed on Kärra clay, ψ scales the impact of the 'overconsolidation ratio' on the magnitude of cyclic accumulated strain. This parameter is related to amplitude dependency and seems to range between 120 and 160 for high and low amplitude tests, respectively. Table 5 presents values of ψ for tests with low and subsequently higher shear mobilisation ratio. Table 6 presents the
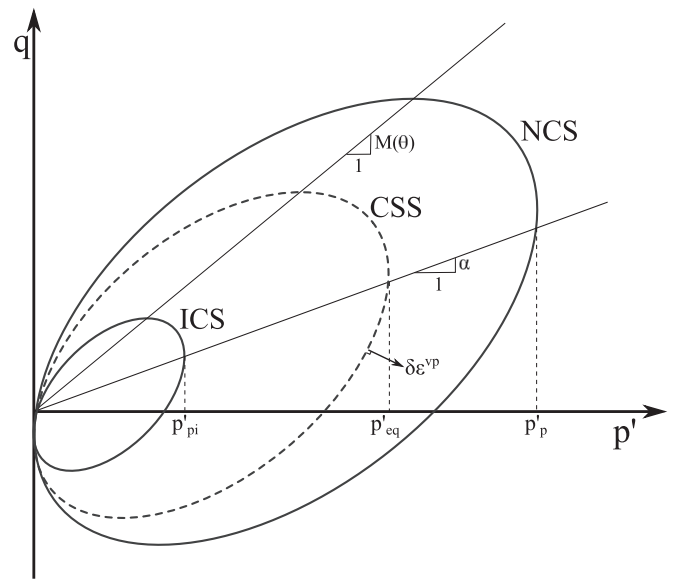
Table 7
Cyclic model parameters of Creep-SCLAY1Sc for Kärra clay.

Parameter	Description	Unit	Value
ζ	Axial strain accumulation factor	-	3.22×10^{-4}
ι	scaling factor for the fraction of cyclic and static loading	-	1.83×10^{-4}
Γ_α	scaling factor of cyclic reference time	-	6.96×10^{-2}
Γ_β	exponential scaling factor of cyclic reference time	-	2.038
Ξ	scaling factor of loading period	-	7.9×10^{-1}

remaining parameters for small-strain formulation, as derived from the experimental data on Kärra in Section 2.

Results

Figs. 9 and 11, show the computed and experimental results of the cyclic stage of the undrained cyclic triaxial tests on Kärra clay. In these figures, the computed and measured mean value of the axial strain is plotted against the corresponding number of loading cycles *N*. All other

numerical properties of the Finite Element model are similar to those discussed in Section 2.3.

Fig. 9 represents the samples with relatively high loading amplitude, *i.e.* the degree of shear mobilisation falls above the empirical failure threshold (the red line shown in Fig. 8). The onset of failure is reached between 3 to 5% of axial strain, as indicated by a very sudden and clear increase in the strain rate in test data; see Fig. 9. The newly introduced Creep-SCLAY1Sc2 model captures the measured response well at low levels of strain because of the implementation of the non-linear small strain formulation. However, an overestimation of axial strain is observed at a large number of loading cycles near the onset of failure. Fig. 10 shows the excess pore water pressures during the undrained cyclic loading stage, *i.e.* developed within Test 08, Test 09, and Test 11. The increase in loading cycles was followed by a subsequent increase in pore water pressure until the onset of failure was reached. Clearly, the proposed model formulation, whilst capturing the accumulated strains, overestimates the shape and magnitudes of the generated excess pore water pressures.

Fig. 11 shows the results of the tests that fall below the empirical failure threshold, *i.e.* tests with low cyclic loading amplitudes. The magnitudes of measured axial strain does not indicate failure. Furthermore, a non-linear relation between axial strain and the number of cycles has been observed at very small axial strains — generally less than about 0.5%. The accumulated axial strain becomes even lower than 0.3% for the experiments without pre-shearing, *i.e.* Tests 05 and 06, as shown in Figs. 11b and 11c.

Similar to large amplitude tests, the increase in loading cycles was accompanied by an increase in pore water pressure, as shown in Fig. 12. The sudden jump in the excess pore water pressures during the initial phase of the simulation might be probably due to increased stiffness response of the model. However, more detailed investigation is required in terms of model interactions with the storage equation of the water flow. In comparison for the tests at large loading amplitudes, a steady state is reached for $q_{cyc} = 5$ kPa at a high number of cycles, in which no further increase in cumulative strain is observed.

Given these results, the comparison between the experimental data and the model predictions are deemed to be reasonable. However, more effort is required to model the stable phase at a higher number of cycles, such as Test 06, where the generation of accumulated strains is stabilising the experiment, despite an ongoing increase in excess pore water pressures, albeit not in the model.

The three tests at low loading amplitudes that had not been brought to failure during the cyclic loading stage, were subsequently monotonically sheared to failure in undrained conditions. A comparison between the model predictions and the results of the three post-cyclic sheared tests is shown in Fig. 13. When compared to the monotonic undrained shear strength, *i.e.* $s_u = q/2 = 33$kPa, the post-cyclic strength did not appreciably change after the cyclic loading stage. A more pronounced softening behaviour, however, is observed for all three cyclic experiments, as opposed to the reference (monotonic) test. The post peak softening could not be fully captured by the numerical analysis given an axisymmetric formulation and only one element was used in the analyses.

Conclusions

A series of undrained cyclic triaxial tests on a natural Swedish clay with high plasticity has been performed at different loading amplitudes. The focus of the test programme was on small loading amplitudes that represent loading conditions below a railway embankment on soft clays. In addition, certain tests incorporated a pre-shearing phase to assess the effects of pre-loading, such as construction of an embankment or excavation, prior to cyclic loading. Undrained pre-shearing has a considerable effect on the rate of accumulated strain, *i.e.* the magnitude of the cyclic resistance R_ϵ reduced substantially with increased pre-shearing.

Regardless, the relation between the cyclic resistance R_ϵ and number of loading cycles is nearly linear, supporting the findings of Janbu [21], and depends on the degree of the shear mobilisation q_{cyc}/p_0' . An exponential relationship between the resistance number m_ϵ and shear mobilisation q_{cyc}/p_0' was established.

The cyclic response of the clay tested at small loading amplitudes is primarily a creep process, but with larger creep rates than can be expected for deviatoric creep alone. The prediction accuracy of the Creep-SCLAY1Sc model, developed for large loading amplitudes, calibrated against the new data set, was quite poor at small loading amplitudes. As a result, a revised strain accumulation model, based on Janbu's resistance concept with an additional function for small strain, was developed to model the cyclic loading of soft natural clay. The model incorporates a cyclic viscoplastic multiplier to account for the strain accumulation induced by cyclic loading, which is similar to the viscoplastic effects that occur due to rate-dependence. As part of the model extension, four new model parameters were introduced which are determined through undrained cyclic triaxial tests and small-strain stiffness measurements. The newly proposed model demonstrated a satisfactory performance in predicting the accumulation of strains for slightly over-consolidated clays, including the Kärra clay studied in this paper. Furthermore, the model accurately accounted for the relationship between the number of repetitions and the resulting accumulated strain response for both low and high amplitude tests performed under repeated loading with constant deviatoric stress changes. The results demonstrate that the proposed model is currently unable to predict the accumulated excess pore water pressures. Therefore, future efforts are necessary to investigate the detailed interactions between the model and the storage equation, which is coupled to the material deformations via the volumetric strain. Additionally, it is necessary to consider the stable phases for low amplitudes at higher numbers of cycles where the strain accumulation becomes stable.

The model presented in this study serves as a solid foundation to simulate strain accumulation under embankments on soft clays subjected to repeated loading cycles. Although the model can simulate many loading cycles in a computationally efficient manner, it needs to be validated at field scales. To this end, the integration of Global Sensitivity Analysis (GSA) techniques with Finite Element modelling can be utilised in the development of design instrumentation and/or monitoring plans [50]. The model validated for larger scales can provide valuable insights for railway infrastructure managers to assess the condition of railway assets and evaluate the impact of traffic operations, such as train speed or traffic loading, on the operational cost of railway infrastructure.

Declaration of Competing Interest

The authors declare that they have no known competing financial interests or personal relationships that could have appeared to influence the work reported in this paper.

Data availability

Data will be made available on request.

Acknowledgements

Brief overview of Creep-SCLAY1Sc

The stress-state of the Creep-SCLAY1Sc model in triaxial space includes three main surfaces that are inclined as defined by the anisotropy scalar α; see Fig. 14. The shape and orientation of all surfaces are similar and defined according to Eq. 22:

$$f_{\text{surface}} = \left(q - \alpha p'\right)^2 - \left(M(\theta)^2 - \alpha^2\right)\left(p'_{\text{surface}} - p'\right)p' = 0 \tag{22}$$

In Eq. 22, M controls the stress ratio at a critical state and is a function of the modified Lode angle θ.

The definition of the three surfaces have been adopted from Gras et al. [14] and is as follows:

- Normal Consolidation Surface (NCS): Defines a boundary surface between the small and large viscoplastic strains. Note that elastic and viscoplastic strains are generated for all stress states and that only the magnitude of the viscoplastic strain rate substantially increases when the current stress is beyond the NCS. The extent of this boundary is established by a preconsolidation pressure projected onto the isotropic axis p'_p.
- Current Stress Surface (CSS): A surface that follows the current state of effective stress and its extent is regulated by the mean effective stress p'_{eq}.
- Intrinsic Compression Surface (ICS): This state represents an imaginary clay sample without bonding but supplied with a similar void ratio and fabric of the NCS surface. The extent of ICS is determined by the intrinsic isotropic preconsolidation pressure p'_{pi}, in which the size of ICS and NCS is interconnected through a bonding parameter χ as expressed in Eq. 23.

$$p'_p = \left(1 + \chi\right)p'_{pi} \tag{23}$$

Subsequently, the model consists of three hardening laws:

1. Volumetric hardening law: It states that the rate of viscoplastic volumetric strain determines the size of the ICS, as indicated in Eq. 24.

$$\dot{p}'_p = \frac{p'_{pi}}{\lambda_i^* - \kappa^*} \cdot \dot{\epsilon}_v^c \tag{24}$$

2. Rotational hardening law: The rotational hardening law accounts for the changing anisotropy by incorporating the rate of the volumetric viscoplastic strain $\dot{\epsilon}_v^c$ and the deviatoric viscoplastic strain $\dot{\epsilon}_d^c$ [52]; see Eq. 25.

$$\dot{\alpha} = \omega\left[\left(\frac{3q}{4p'} - \alpha\right)\langle\dot{\epsilon}_v^c\rangle + \omega_d\left(\frac{q}{3p'} - \alpha\right)|\dot{\epsilon}_d^c|\right] \tag{25}$$

3. Destructuration hardening law: Eq. 26 takes into account the degradation of the bonding through the introduction of two parameters, namely the absolute and relative rate of destructuration (a & b). Under this assumption, both the volumetric and deviatoric viscoplastic strains reduce the bonding parameter χ until it ultimately reaches zero, signifying an irreversible degradation of the initial bonding [24].

$$\dot{\chi} = -a\chi\left(|\dot{\epsilon}_v^c| + b|\dot{\epsilon}_d^c|\right) \tag{26}$$

The constitutive model adopts a similar division of strains as in Eq. 9, where the viscoplastic component in Eq. 9 is specified as:

$$\dot{\epsilon}_{ij}^{vp} = \left[\dot{\Omega} + \dot{\Lambda}\right]\frac{\partial p'_{eq}}{\partial \sigma'_{ij}} \tag{27}$$

in which $\dot{\Lambda}$ is the rate-dependent viscoplastic multiplier that is defined similarly as in Eq. 11. The cyclic accumulation multiplier $\dot{\Omega}$ in Eq. 28 consists of three normalised terms: the first term represents the gradient of the cyclic axial strain, the second component controls the model's dependence on frequency, and the third component captures the influence of loading amplitude [59].

$$\dot{\Omega} = \underbrace{\frac{\zeta}{t_{\text{ref}|0.1\%}}}_{i}\underbrace{\left(\frac{T}{T_0}\right)^{\Xi}}_{ii}\underbrace{\left(\frac{q_{\text{cyc}}}{p'M(\theta) - q}\right)^{\iota}}_{iii} \tag{28}$$

and $t_{\text{ref}|0.1\%}$, *i.e.* the cyclic reference time at 0.1% of deviatoric strain, is defined in Eq. 29:

$$t_{\text{ref}|0.1\%} = \Gamma_\alpha\left(\frac{q_{\text{cyc}}}{p'_0}\right)^{-\Gamma_\beta} \tag{29}$$

T_0 and T in Eq. 28 denote the reference and current loading period, respectively. q_{cyc} is the cyclic deviatoric stress, $M(\theta)$ the critical state stress ratio, p' the current mean effective stress, and q the current deviatoric stress. Moreover, p'_0 stated in Eq. 29 is the initial mean effective stress. The five model parameters of Creep-SCLAY1Sc and their corresponding values for Kärra clay are summarised in Table 7. The remaining parameters are the same as Table 3. For a comprehensive understanding of Creep-SCLAY1Sc, the reader is referred to Zuada Coelho et al. [59]; Gras et al. [14]; Sivasithamparam et al. [44].

References

[1] Abadi T, Le Pen L, Zervos A, Powrie W. A review and evaluation of ballast settlement models using results from the southampton railway testing facility (srtf). Proc Eng 2016;143:999–1006.

[2] Andersen KH. Bearing capacity under cyclic loading–offshore, along the coast, and on land. the 21st bjerrum lecture presented in oslo, 23 november 2007. Can Geotech J 2009;46(5):513–35.

[3] Ansal AM, Erken A. Undrained behavior of clay under cyclic shear stresses. J Geotech Eng 1989;115(7):968–83.

[4] Bishop AW, Wesley LD. A hydraulic triaxial apparatus for controlled stress path testing. Géotechnique 1975;25(4):657–70.

[5] Cao Z, Chen J, Ye X, Gu C, Guo Z, Cai Y. Experimental study on particle breakage of carbonate gravels under cyclic loadings through large-scale triaxial tests. Transport Geotech 2021;30:100632.

[6] Carter M, Bentley SP. Soil properties and their correlations. John Wiley & Sons; 2016.

[7] Chen C, Xu G, Zhou Z, Kong L, Zhang X, Yin S. Undrained dynamic behaviour of peaty organic soil under long-term cyclic loading, part ii: Constitutive model and simulation. Soil Dynam Earthquake Eng 2020;129. https://doi.org/10.1016/j.soildyn.2019.01.039.

[8] Chen J, Alonso EE, Gu C, Cao Z, Cai Y. Long term cyclic behavior of unsaturated granular soils. Transport Geotech 2018;17:48–55.

[9] Darendeli MB. Development of a new family of normalized modulus reduction and material damping curves. The university of Texas at Austin; 2001. PhD thesis.

[10] Dijkstra J, Tahershamsi H, Ahmadi-Naghadeh R. Degradation of a natural sensitive clay under cyclic loading. Sweden: Chalmers University of Technology; 2022. Technical report.

[11] Duque J, Roháč J, Mašín D, Najser J. Experimental investigation on malaysian kaolin under monotonic and cyclic loading: inspection of undrained miner's rule and drained cyclic preloading. Acta Geotech 2022;17(11):4953–75.

[12] Einav I. Breakage mechanics–part ii: Modelling granular materials. J Mech Phys Solids 2007;55(6):1298–320.

[13] Gras J-P, Sivasithamparam N, Karstunen M, Dijkstra J. Strategy for consistent model parameter calibration for soft soils using multi-objective optimisation. Comput Geotech 2017;90:164–75. ISSN 0266352X.

[14] Gras J-P, Sivasithamparam N, Karstunen M, Dijkstra J. Permissible range of model parameters for natural fine-grained materials. Acta Geotech 2018;13(2):387–98.

[15] Grimstad G, Degago SA, Nordal S, Karstunen M. Modeling creep and rate effects in structured anisotropic soft clays. Acta Geotech 2010;5(1):69–81.

[16] Grossoni I, Powrie W, Zervos A, Bezin Y, Le Pen L. Modelling railway ballasted track settlement in vehicle-track interaction analysis. Transport Geotech 2021;26: 100433.

[17] Guo Y, Zhao C, Markine V, Jing G, Zhai W. Calibration for discrete element modelling of railway ballast: A review. Transport Geotech 2020;23:100341.

[18] Hardin BO, Drnevich VP. Shear modulus and damping in soils: design equations and curves. J Soil Mech Found Divis 1972;98(7):667–92.

[19] Indraratna B, Lackenby J, Christie D. Effect of confining pressure on the degradation of ballast under cyclic loading. Geotechnique 2005;55(4):325–8.

[20] Janbu N. The resistance concept applied to deformations of soils. In Proceedings of the 7th international conference on soil mechanics and foundation engineering, 1, pages 191–196, Mexico city, 1969.

[21] Janbu N. Soils under cyclic loading. In: Proceedings of the first international conference BOSS'76; 1976. p. 373–385.

[22] Janbu N. Soil models in offshore engineering. Géotechnique 1985;35(3):241–81. https://doi.org/10.1680/geot.1985.35.3.241.

[23] Jardine RJ, Potts DM, Fourie AB, Burland JB. Studies of the influence of non-linear stress–strain characteristics in soil–structure interaction. Géotechnique 1986;36(3): 377–96. https://doi.org/10.1680/geot.1986.36.3.377.

[24] Karstunen M, Krenn H, Wheeler SJ, Koskinen M, Zentar R. Effect of anisotropy and destructuration on the behavior of murro test embankment. Int J Geomech 2005;5 (2):87–97. https://doi.org/10.1061/(ASCE)1532-3641(2005)5:2(87).

[25] Leroueil S, Vaughan PR. The general and congruent effects of structure in natural soils and weak rocks. Géotechnique 1990;40(3):467–88.

[26] Li D, Selig ET. Cumulative plastic deformation for fine-grained subgrade soils. J Geotech Eng 1996;122(12):1006–13. https://doi.org/10.1061/(ASCE)0733-9410(1996)122:12(1006).

[27] Li L-L, Dan H-B, Wang L-Z. Undrained behavior of natural marine clay under cyclic loading. Ocean Eng 2011;38(16):1792–805.

[28] Li T, Meissner H. Two-surface plasticity model for cyclic undrained behavior of clays. J Geotech Geoenviron Eng 2002;128(7):613–26. https://doi.org/10.1061/(ASCE)1090-0241(2002)128:7(613).

[29] Liu HY, Abell JA, Diambra A, Pisanò F. Modelling the cyclic ratcheting of sands through memory-enhanced bounding surface plasticity. Géotechnique 2019;69(9): 783–800.

[30] Lobo-Guerrero S, Vallejo LE. Discrete element method analysis of railtrack ballast degradation during cyclic loading. Granul Matter 2006;8(3):195–204.

[31] Lopez-Pita A, Teixeira PF, Casas C, Bachiller A, Ferreira PA. Maintenance costs of high-speed lines in Europe state of the art. Transport Res Rec 2008;2043(1):13–9.

[32] Lu M, McDowell GR. Discrete element modelling of railway ballast under monotonic and cyclic triaxial loading. Géotechnique 2010;60(6):459–67.

[33] Mitchell JK, Soga K. Fundamentals of Soil Behavior. 3 edition. Wiley; 2005.

[34] Mróz Z, Norris VA, Zienkiewicz OC. An anisotropic hardening model for soils and its application to cyclic loading. Int J Numer Anal Meth Geomech 1978;2(3): 203–21.

[35] Ni J, Indraratna B, Geng X, Carter J, Chen Y. Model of soft soils under cyclic loading. Int J Geomech 2014;15(4):1–10. https://doi.org/10.1061/(ASCE) GM.1943-5622.0000411.

[36] Niemunis A, Wichtmann T, Triantafyllidis Th. A high-cycle accumulation model for sand. Comput Geotech 2005;32(4):245–63.

[37] Powrie W, Le Pen L, Milne D, Thompson D. Train loading effects in railway geotechnical engineering: Ground response, analysis, measurement and interpretation. Transport Geotech 2019;21:100261.

[38] Qian J-G, Wang Y-G, Yin Z-Y, Huang M-S. Experimental identification of plastic shakedown behavior of saturated clay subjected to traffic loading with principal stress rotation. Engineering Geology 2016;214:29–42. https://doi.org/10.1016/j.enggeo.2016.09.012. ISSN 0013–7952.

[39] Roberts WJ, Romine HE. Effect of train loading on the water level in a deep glacial-drift well in central illinois. Eos, Trans Am Geophys Union 1947;28(6):912–7.

[40] Sangrey DA, Henkel DJ, Esrig MI. The effective stress response of a saturated clay soil to repeated loading. Can Geotech J 1969;6(3):241–52.

[41] Selig ET, Li D. Track modulus: Its meaning and factors influencing it. Transportation research record 1994;1470:47–54.

[42] SGF. Metodbeskrivning för provtagning med standardkolvprovtagare - ostörd provtagning i finkornig jord. Stockholm: Swedish Geotechnical Society; 2009. Technical Report 1.

[43] Sivasithamparam N, D'Ignazio M, Tsegaye AB, Castro J, Madshus C. Small strain stiffness within logarithmic contractancy model for structured anisotropic clay. In: IOP Conference Series: Earth and Environmental Science, volume 710. IOP Publishing; 2021. p. 012042.

[44] Sivasithamparam N, Karstunen M, Bonnier P. Modelling creep behaviour of anisotropic soft soils. Comput Geotech 2015;69:46–57. https://doi.org/10.1016/j.compgeo.2015.04.015. ISSN 18737633.

[45] Staubach P, Machaček J, Tafili M, Wichtmann T. A high-cycle accumulation model for clay and its application to monopile foundations. Acta Geotech 2022;17(3): 677–98.

[46] Suiker ASJ, de Borst R. A numerical model for the cyclic deterioration of railway tracks. Int J Numer Methods Eng 2003;57(4):441–70.

[47] Suiker ASJ, Selig ET, Frenkel R. Static and cyclic triaxial testing of ballast and subballast. J Geotech Geoenviron Eng 2005;131(6):771–82.

[48] Sällfors G. Preconsolidation pressure of soft, high-plastic clays. PhD thesis, 1975.

[49] Tafili M, Triantafyllidis T. AVISA: anisotropic visco-isa model and its performance at cyclic loading. Acta Geotech 2020;15:2395–413. https://doi.org/10.1007/ s11440-020-00925-9.

[50] Tahershamsi H, Dijkstra J. Using experimental design to assess rate-dependent numerical models. Soils Found 2022;62(6):101244. https://doi.org/10.1016/j. sandf.2022.101244. ISSN 0038–0806.

[51] Wang J, Guo L, Cai Y, Xu C, Gu C. Strain and pore pressure development on soft marine clay in triaxial tests with a large number of cycles. Ocean Eng 2013;74: 125–32.

[52] Wheeler SJ, Näätänen A, Karstunen M, Lojander M. An anisotropic elastoplastic model for soft clays. Can. Geotech. J. 2003;40(2):403–18.

[53] Wichtmann T. Explicit accumulation model for non-cohesive soils under cyclic loading. Ruhr-University Bochum; 2005. PhD thesis.

[54] Wichtmann T, Andersen KH, Sjursen MA, Berre T. Cyclic tests on high-quality undisturbed block samples of soft marine norwegian clay. Can Geotech J 2013;50 (4):400–12.

[55] Wood T. On the Small Strain Stiffness of Some Scandinavian Soft Clays and Impact on Deep Excavations. Chalmers University of Technology; 2016. PhD thesis.

[56] Xiao Y, Meng M, Daouadji A, Chen Q, Wu Z, Jiang X. Effects of particle size on crushing and deformation behaviors of rockfill materials. Geosci Front 2020;11(2): 375–88.

[57] Zhai WM, Wang KY, Lin JH. Modelling and experiment of railway ballast vibrations. J Sound Vib 2004;270(4–5):673–83.

[58] Zhou J, Gong X. Strain degradation of saturated clay under cyclic loading. Can Geotech J 2001;38(1):208–12.

[59] Zuada Coelho B, Dijkstra J, Karstunen M. Viscoplastic cyclic degradation model for soft natural soils. Comput Geotech 2021;135:104176.

[60] Zuada Coelho B, Varandas JN, Hijma MP, Zoeteman A. Towards network assessment of permanent railway track deformation. Transport Geotech 2021;29: 100578.